Ground Water Monitoring&Remediation

Spatial Variability of Soil-Gas Concentrations near and beneath a Building Overlying Shallow Petroleum Hydrocarbon–Impacted Soils

by Hong Luo, Paul Dahlen, Paul C. Johnson, Tom Peargin, and Todd Creamer

Abstract

Data requirements for assessing the significance of the soil vapor intrusion pathway are evolving, and the collection and interpretation of subslab and near-slab soil-gas samples are under discussion. The potential for different assessment paradigms for aerobically biodegradable and recalcitrant chemicals is also frequently debated. In this work, the soil-gas distribution beneath and around a slab-on-grade building overlying shallow (0.5 to >1.5 m below ground surface) petroleum hydrocarbon–impacted coarse alluvial soils was studied. The study spanned about 12 months, including the sampling of soil-gas hydrocarbon and oxygen concentrations, subslab soil vs. building pressure differentials and included weather conditions. Three-dimensional soil-gas concentration "snapshots" using samples from 79 soil-gas sampling points are presented here. Significant spatial variability was observed with hydrocarbon and oxygen concentrations ranging from about <0.01 to 200 mg/L and 0 to 21% v/v, respectively. The presence of oxygen and the depth to petroleum-impacted soils appeared to be the dominant factors in controlling the soil-gas distribution; the depletion of hydrocarbons over short lateral and vertical distances (<2 m) was observed in the well-oxygenated regions. Composition data suggest preferential biodegradation of lighter compounds at some points, as reflected in the ratio of the masses of chemicals eluting on the gas chromatography between methane and pentane (C1 and C5) and all others after pentane (>C5).

Introduction

Recognition of subsurface soil vapor intrusion to buildings and other enclosed spaces as an exposure pathway to indoor air occurred in the 1980s with concerns over radon intrusion (Nazaroff et al. 1985, 1987). In the 1990s, there was an increasing awareness that anthropogenic chemicals (e.g., petroleum hydrocarbons and chlorinated solvents) in soil and ground water could also pose threats to indoor air quality (Little et al. 2002; Fischer et al. 1996; Fitzpatrick and Fitzgerald 2002). More recently, this exposure pathway has been of considerable interest to regulatory agencies. For example, the U.S. Environmental Protection Agency (USEPA), about 20 states, and several industry groups have developed pathway assessment guidance documents (USEPA 2002, 2004). Most employ a version of the multiple-lines-of-evidence approach favored by USEPA. In that approach, some combination of ground water, deep soil-gas, subslab soil-gas, and indoor air concentrations is considered in assessing current and future vapor intrusion impacts to indoor air. Extrapolation from subsurface to indoor air concentrations is required for soil-gas and ground water data, and this generally involves the use of empirical attenuation factors and screening-level modeling (Johnson and Ettinger 1991; Fitzpatrick and Fitzgerald 2002; Johnson et al. 2002; Hers et al. 2002). Inherent in this approach is an assumption that the measured concentrations are sufficiently representative of the subsurface conditions. This naturally raises questions concerning the numbers of sampling locations and sampling events, and little information on which to base these decisions is available in the literature.

In addition, there is debate concerning the need for subslab measurements given that this generally involves drilling holes through foundations and disrupting the homeowners' lives (USEPA 2002, 2004). Some have proposed sampling adjacent to foundations (near-foundation sampling) as a substitute for subslab sampling. Again, little information with which to assess the merit of this proposal is available in the literature.

Our understanding of soil-gas distributions beneath and near foundations at petroleum hydrocarbon–impacted sites stems mainly from anecdotal site studies and mathematical modeling. For example, Laubacher et al. (1997) present data from five multidepth soil-gas monitoring clusters

Copyright © 2009 The Author(s)
Journal compilation © 2009 National Ground Water Association.

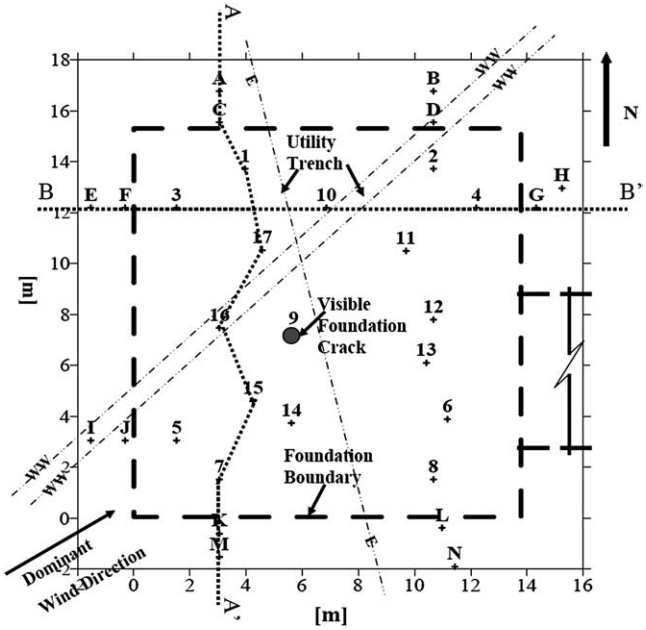

Figure 1. Plan view of building foundation showing soil-gas sampling and pressure monitoring locations (numbered and lettered "+" locations) and alignment of soil-gas cross-sections A-A' and B-B' presented in Figures 7 and 8. Dashed lines "WW" and "E" indicate the approximate location of the shallow (<4 feet bgs) wastewater and electric utility trenches respectively.

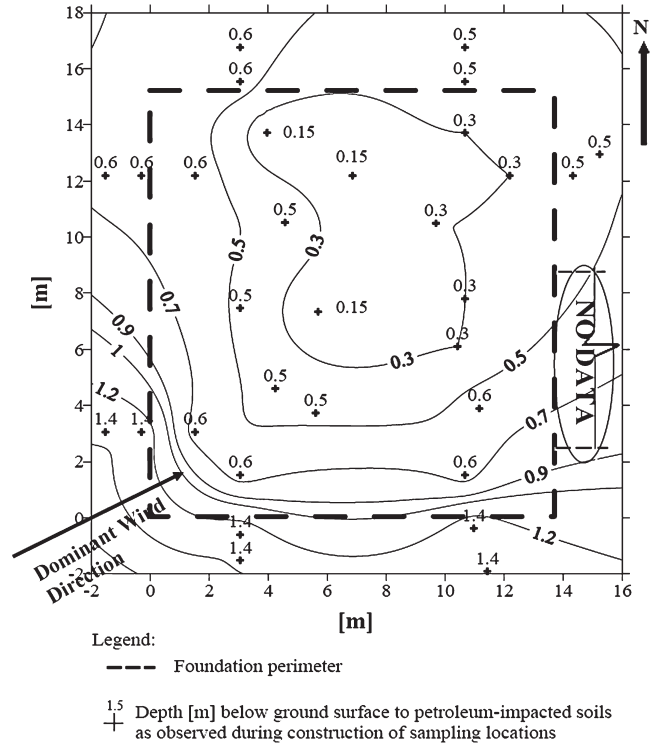

Figure 2. Depth (m) to the top of the hydrocarbon-impacted soils as determined by visual staining and odor. Note: any source zone depth > 1.4 m is shown as a depth of 1.4 m for contouring purposes because investigations were limited to 1.4 m bgs.

installed at a residence having about a 40 m^2 footprint and overlying a gasoline-impacted aquifer. Three of the soil-gas sampling clusters were installed through the foundation and two were installed exterior to the building. Little difference in soil-gas composition was observed laterally or vertically beneath the foundation; the soil-gas had elevated total petroleum hydrocarbon (TPH) and depleted O_2. At locations near but exterior to the foundation, there was also little lateral variation in composition, but the soil-gas TPH concentration decreased in the upward vertical direction by about an order of magnitude from 4.9 to 1.3 m (16 to 4 feet) below ground surface (bgs). Also, the TPH concentration in exterior shallow soil-gas samples (< 2.4 m bgs) was roughly an order of magnitude lower than concentrations beneath the building foundation. The authors attributed the differences in soil-gas composition beneath and adjacent to the foundation to a combination of aerobic biodegradation

Table 1
Sampling Capabilities for Each Sampling Location

—	Sampling Locations	Sampling Point Depths (m bgs)	Sampling Capabilities: Soil-Gas Sampling	Real-Time O_2 Monitoring	Real-Time Soil-to-Indoor Pressure Differential ($\Delta P_{soil\text{-}indoor}$) Monitoring	Real-Time Lateral Pressure Differential ($\Delta P_{lateral}$) Monitoring
Beneath foundation	#1–#17	0.15	Yes	—	—	—
		0.6	Yes	Yes	Yes	—
		1.2	Yes	Yes	—	—
	#1 and #7	—	—	—	—	Yes
	#2 and #8	—	—	—	—	Yes
	#5 and #6	—	—	—	—	Yes
	#3 and #4	—	—	—	—	Yes
Exterior to foundation	A,B,E,H,I,M,N	0.6	Yes	—	Yes	—
		1.2	Yes	—	—	—
	C,D,F,G,J,K,L	0.6	Yes	—	—	—
		1.2	Yes	—	—	—

Table 2
Site Conditions during the Two Sampling Events

	Average Ambient Temperature (°C)	Average Wind Speed (m/s)	Dominant Wind Direction (degrees)	Cumulative Precipitation over Previous 2 Weeks (mm)	Surface Cover
Sampling event 1, September 12–14	11.3	3.8	250	5.0	No change
Sampling event 2, January 3–5	4.65	5.1	242	5.2	No change

and atmospheric O_2 transport limitations caused by building foundation. Hers and Zapf-Gilje (1998) measured soil--gas composition around a constructed greenhouse (about a 60 m^2 footprint) at a former petrochemical plant and found that subslab soil-gas concentrations at one of the four locations was about 100 times greater than those at the other three locations. Hers and Zapf-Gilje (1998) postulated that this was due to lateral variations in soil moisture below the building slab. McAlary et al. (2007) measured soil-gas about an office building (about a 75 m^2 footprint) at a former oil refinery site. Samples were collected from 11 subslab and four outdoor multidepth sampling locations. It was found that the O_2 levels in subslab soil gas were about 2% v/v except for one subslab location. The TPH concentrations ranged from nondetect to about 2 mg/L. There was no significant TPH or O_2 concentration difference laterally between the only two exterior locations, but vertically the TPH increased by about 1000 times from 1.8 to 2.7 m bgs (6 to 9 feet). The authors suggested that the vertical soil-gas profile reflects aerobic biodegradation.

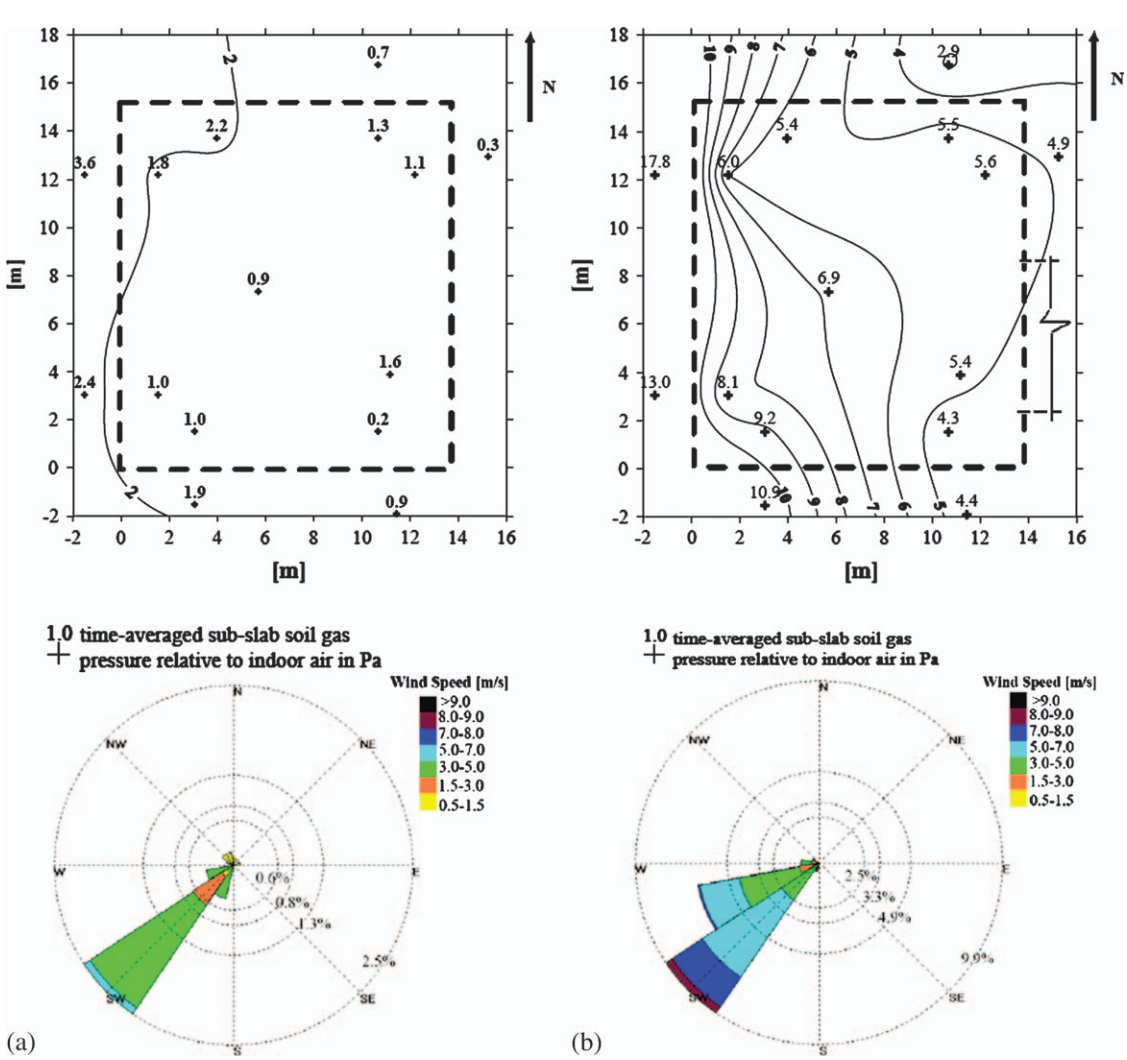

Figure 3. Wind rose and time-averaged subslab soil-gas pressure relative to indoor air ($\Delta P_{soil\text{-}indoor}$) during the two soil-gas sampling events: (a) mid-September and (b) early January 4 months later. Note: during data collection time period, the building was open during the day, closed during the night, and heating was used only as necessary during the day.

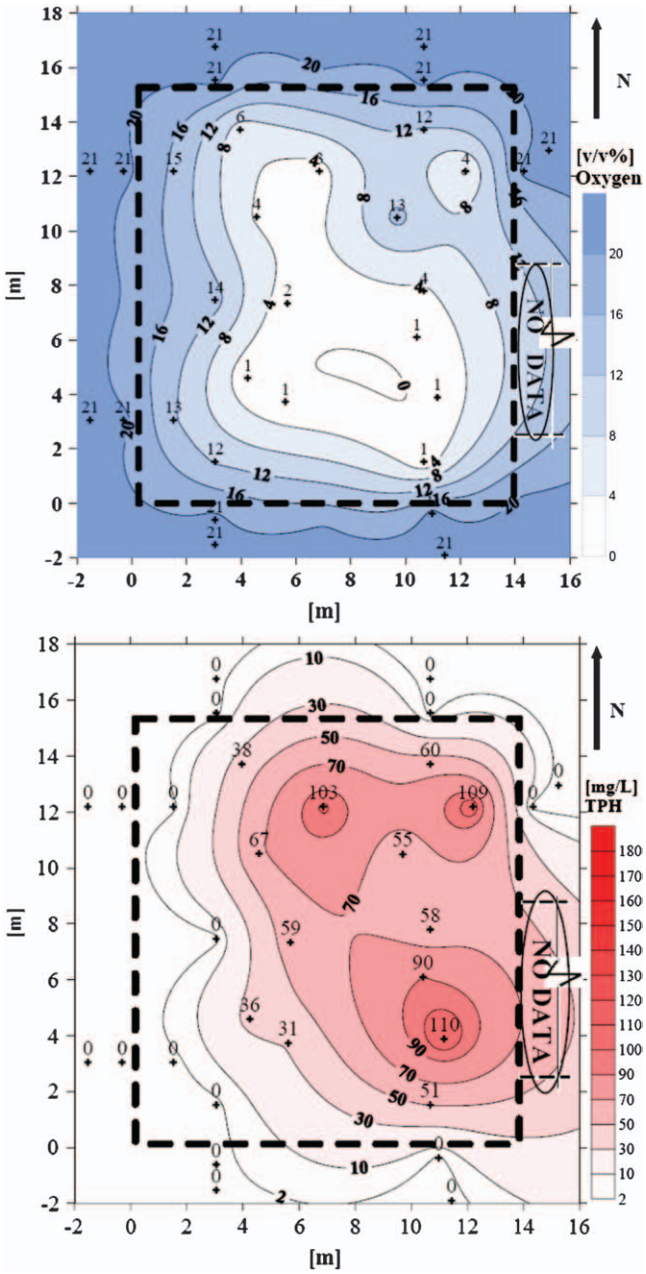

Figure 4. O_2 and TPH subslab depth (0.15 m [0.5 feet] bgs) soil-gas concentrations.

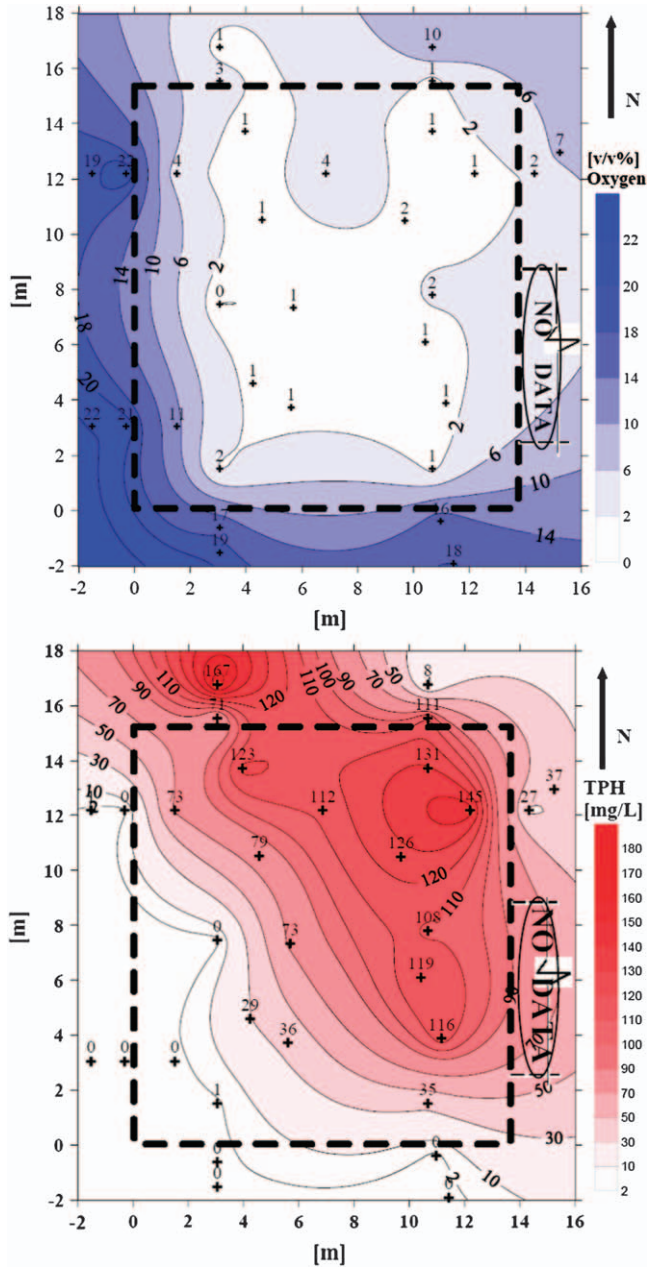

Figure 5. O_2 and TPH soil-gas distribution at 0.6 m (2 feet) bgs.

Soil-gas distributions and the factors that affect them have been anticipated by complex three-dimensional numerical codes (Abreu and Johnson 2005, 2006). For example, Abreu and Johnson (2006) concluded that significant attenuation with depth can occur beneath and adjacent to foundations, provided there is sufficient atmospheric O_2 replenishment to the subsurface. In the absence of O_2 replenishment beneath a foundation, little attenuation with depth or horizontal position was observed in their simulations involving laterally extensive sources in homogeneous soils. Overall, the published modeling results have not shown significant lateral concentration changes immediately beneath foundations. This may in part be due to the use of laterally extensive, uniform depth, and constant concentration vapor sources coupled with homogeneous soil settings. Even in those settings, however, significant differences between subslab and exterior samples have been predicted (Abreu and Johnson 2005, 2006).

Given the significance of soil-gas sampling in pathway assessment guidance as discussed previously, it is important to gain a better understanding of soil-gas distributions and factors affecting them beneath and adjacent to buildings. In this study, the soil-gas concentration distribution near and beneath a slab-on-grade warehouse overlying petroleum-impacted soils was monitored with high spatial and temporal resolution using data collected from 31 locations and three depths. Soil-gas composition, characterized by TPH and O_2, was quantified during two sampling events (or soil-gas snapshots). In addition, soil-gas O_2 concentrations and soil-gas pressures near and beneath the warehouse foundation and weather conditions (wind speed, wind

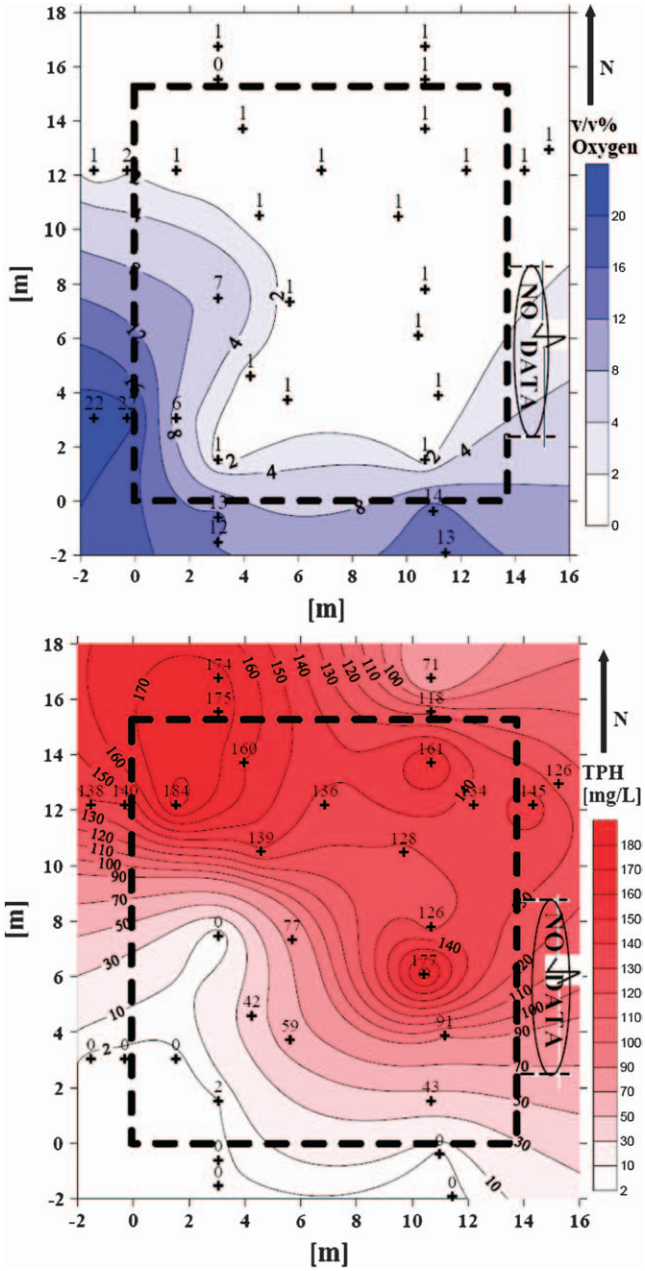

Figure 6. O_2 and TPH soil-gas distribution at 1.2 m (4 feet) bgs.

direction, temperature) were monitored continuously over a year using electronic sensors and a data-logging system. The data provide insight to spatial variability beneath and near foundations overlying impacted soils and they have implication for soil-gas sampling plans for pathway assessment.

Site Description

The study site is a maintenance warehouse located at a former refinery in Evansville, Wyoming. The building dimensions are approximately 15 × 14 m (50 × 45 feet), and the foundation is a slab-on-grade concrete slab that is about 12.5 cm thick. As shown in Figure 1, utility trenches for wastewater and electricity piping run beneath the building and there is a visible, full-thickness crack in the foundation (slab) that is centrally located in the building. The wastewater piping trench is backfilled with gravel having an air permeability of about 1×10^{-9} m^2, measured in the laboratory. The construction details of the electric utility trench are not known. The geology from about 0 to 2 m bgs is predominantly silty medium to fine sands with air permeability of about 5×10^{-12} to 5×10^{-10} m^2. The area surrounding the building is predominantly barren ground with vegetative groundcover limited to native grasses within 1.5 m (5 feet) of the southern side of the building. The building was not airtight when doors and windows were closed, and frequently doors were left open during the day for ventilation.

Because of decades of oil refinery operations and ground water table depth changes from the 0.6 m (2 feet) bgs historical level to the current 4.3 m (14 feet) bgs level, residual light-end petroleum distillates (e.g., gasoline-range petroleum hydrocarbons) are smeared across the shallow soils. These hydrocarbon-impacted soils are a vapor source, and odors are frequently detected in the warehouse after brief periods of being closed. Figure 2 is a contour map showing the depth to the top of the residual hydrocarbon-impacted soils based on the presence of gray/black petroleum hydrocarbon staining and strong hydrocarbon odors in soil samples collected during drilling and installation of the multidepth soil-gas monitoring locations. Hydrocarbon-impacted soils were detected at depths as shallow as 0.15 m (0.5 feet) beneath the foundation of the building and as deep as 1.37 m (4.5 feet) outside the southwestern corner of the building. In general, the depth to hydrocarbon-impacted soils decreases from the southwest to the northeast beneath the building.

Experimental Methods

The 31 multidepth monitoring locations shown in Figure 1 were chosen to yield a good understanding of the soil-gas composition and pressure distribution, after considering the construction of the foundation, known subsurface features, and physical constraints. Slightly more than half of the multidepth clusters (17) (referred to as interior sampling locations) were installed through the foundation and the other 14 (referred to as exterior sampling locations) were installed near but outside of the foundation. Each interior sampling location was constructed to monitor three depths (subslab, 0.6, and 1.2 m bgs) and each exterior sampling location was constructed to monitor two depths (0.6 and 1.2 m bgs). These were constructed using polyethylene tubing, sintered stone diffusers at the end of each section of tubing, sandpacks about each sampling depth, and bentonite seals between each sampling depth. Each sampling location was constructed to allow soil-gas sampling and soil-gas pressure monitoring, as desired. Co-located at all 0.6- and 1.2-m depths were real-time O_2 sensors (USA Figaro Model KE-50, detection range: 0 to 100%, measurement accuracy: ±2%). When used for soil-gas pressure monitoring, differential pressure sensors were employed (Pace Scientific P300, detection range: ±249 Pa, measurement accuracy: ±2% of full scale). Table 1 summarizes the monitoring at each sampling location.

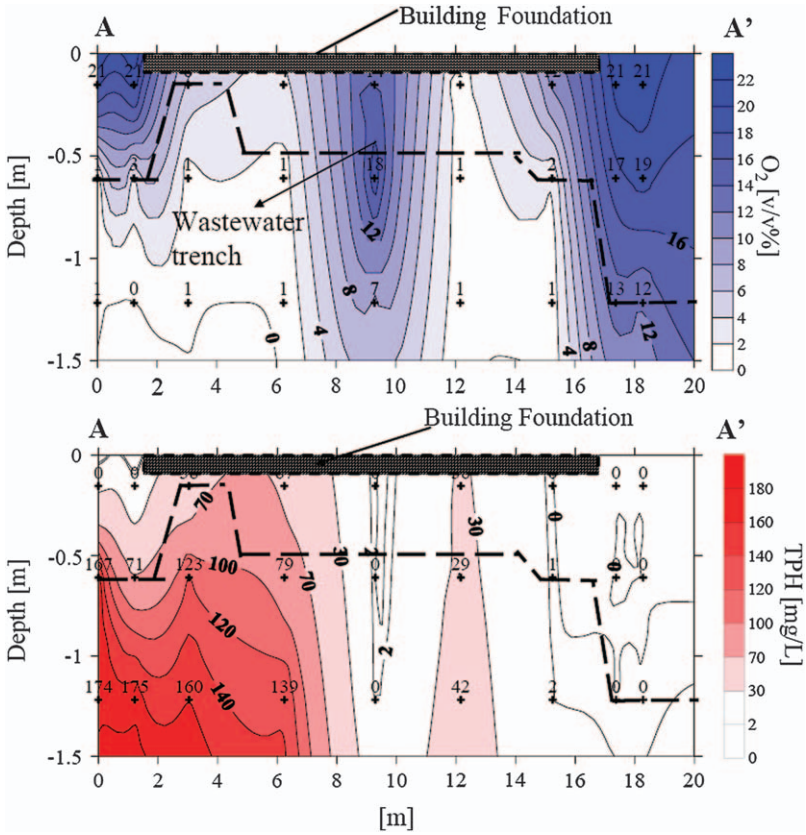

Figure 7. O_2 and TPH soil-gas distribution for vertical cross-section A-A'. Dashed lines beneath building foundation are the estimated source zone depth.

2Instantaneous readings from the oxygen sensors and pressure transducers were logged on 10-min intervals using data acquisition modules (Omega OMB-DAQ-55 and OMB-DAQ-56, resolution: 22-bit). Instantaneous meteorological data readings were collected on 10-min intervals from a station (Onset Computer Corporation Model H21-SYS-A) installed within 45 m (150 feet) of the warehouse.

Real-time data quality was monitored and maintained as follows: pressure transducers were rezeroed monthly and O_2 sensor data were checked against gas chromatography O_2 data in soil-gas samples collected during site.

For site snapshot, soil-gas samples were collected in Tedlar bags by placing the bag in a vacuum box and connecting it to the sampling port, so that the vapors did not pass through a pump. Samples were analyzed within 48 hours of collection. Analyses included TPH, TPH composition as defined by carbon range speciation, O_2, CO_2, and CH_4 using gas chromatography (GC; SRI model 8610C equipped with vapor auto-sampling loop) with flame ionization (FID) and thermal conductivity (TCD) detectors. The TPH calibration was performed using n-alkane standards from methane through decane, and calculating an average response factor. These methods had quantitation limits of about 0.01 mg/L with the FID detector for each n-alkane in the calibration mixture, and about 0.1 v/v% for O_2, CO_2, and CH_4 with the TCD detector.

Results and Discussion

Sampling and GC/FID/TCD analyses of all soil-gas sampling locations were performed twice, with about four months between events. This involved collecting samples from each depth (0.5 feet bgs (subslab), 0.6 m or 2 feet bgs, and 1.2 m or 4 feet bgs) at the 31 soil-gas monitoring locations shown in Figure 1. Because the overall spatial distribution of O_2 and TPH concentration were similar for both events, only the data from the first are presented here. The soil-gas GC/FID/TCD results were also used to verify that the in situ O_2 sensors were operating correctly. A strong correlation exists between the data from both measurement approaches ($r^2 = 0.959$), and those results are presented in Supplemental Information Figure S1.

The first sampling event took place in early fall (September), and the second event took place approximately four months later in midwinter (January). Site conditions during the two sampling events, including ambient temperature, wind speed and direction, surface cover, and precipitation over the previous 2 weeks, are summarized in Table 2. The most significant difference between the two events was the daily average ambient temperature (11°C vs. 4°C). Figures 3a and 3b present wind rose diagrams and shallow soil-gas pressure distributions (the differential pressure relative to indoor air) for both events. In general, both figures show conditions typical of the site; the

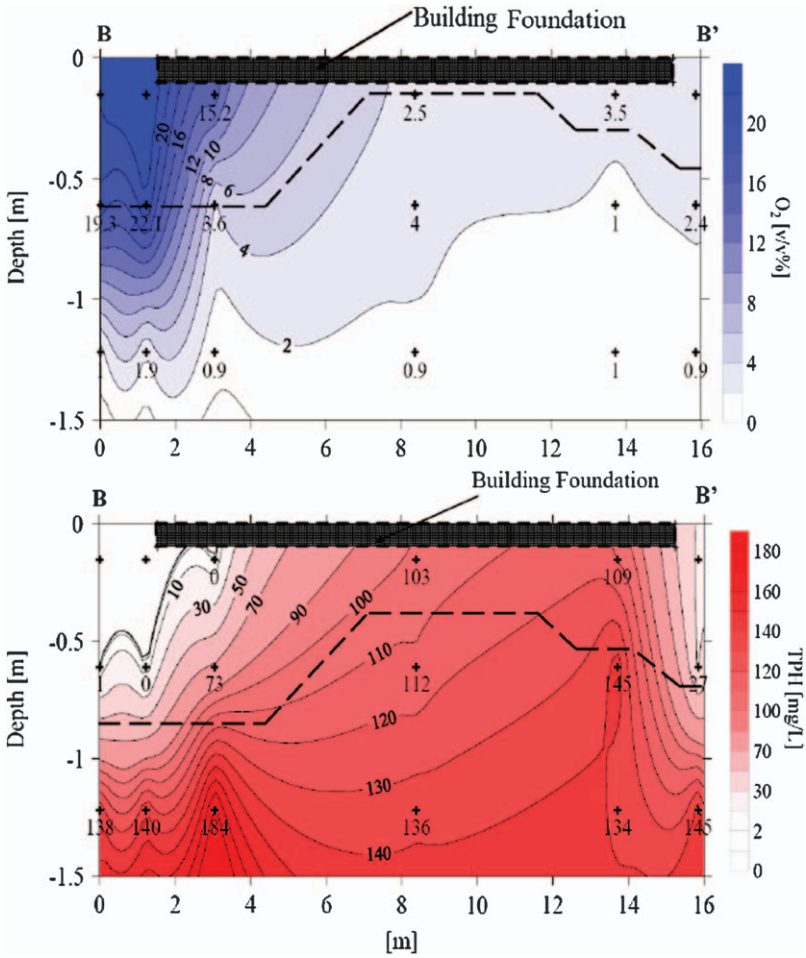

Figure 8. O_2 and TPH soil-gas distribution for vertical cross-section B-B'. Dashed lines beneath building foundation are the estimated source zone depth.

dominant wind direction is from the southwest with wind speeds ranging from 1 to 9 m/s. The soil-gas pressures in these figures indicate that the subsurface is on average at a higher pressure than the warehouse. However, there is no clear pressure gradient and soil-flow direction in Figure 3a and the values are mostly within instrumental error. There is a wind-induced lateral soil-gas pressure gradient of 0.1 Pa/m from the west side to the east side of the foundation in January. Using that gradient, the range of measured soil permeability (5×10^{-12} to 5×10^{-10} m^2), an air-filled porosity estimate of 0.3 cm^3 voids/cm^3 soil, and a soil-gas viscosity estimate of 1.8×10^{-4} g/cm-s, one can estimate average linear soil-gas velocities on the order of 0.1 to 10 cm/d.

Figures 4, 5, and 6 present soil-gas O_2 and TPH concentration contour plots for the subslab (0.15-m bgs), 0.3-m bgs (2-feet), and 0.6-m bgs (4-feet) depths, respectively. The subslab depth contour plots were prepared by treating the region outside the foundation as having 21% v/v O_2 and 0 mg/L TPH in soil-gas because the subslab depth corresponds to ground surface outside of the slab. Figures 7 and 8 present corresponding vertical contour plots along the two transects defined in Figure 1.

These figures show a soil-gas distribution with significant spatial variability. Overall, O_2 concentrations range from <1% v/v to near-atmospheric conditions and TPH concentrations range from nondetect (0.01 mg/L) to about 180 mg/L. The highest TPH concentrations are generally found at those locations and depths where soil-gas was drawn from within the hydrocarbon-impacted soils and in locations below the foundation where O_2 is depleted in the soil gas. Depleted O_2 concentrations are observed at most locations and depths, except outside the foundation and at subslab depths near the south and west foundation edges.

Soil-gas contours for cross-section B-B in particular (Figure 8), and Figures 2 and 5 through 8 in general, suggest that the depth to the hydrocarbon-impacted soils and oxygen supply are the controlling factors in determining the hydrocarbon soil-gas distribution beneath the foundation. The highest subslab soil-gas TPH concentrations are observed in regions where the petroleum hydrocarbon–impacted soils are shallowest and O_2 is depleted. Conversely, the lowest TPH concentrations are observed in the southwest quadrant where the depth to petroleum hydrocarbon–impacted soils is greatest and O_2 concentrations are elevated. As discussed previously, the dominant wind direction at this site is from the southwest, and it is possible that this may be the cause of the increased depth to hydrocarbon-impacted soils in the southwest corner of the foundation (i.e., the higher wind-driven O_2 supply may have resulted in

preferential biodegradation and petroleum hydrocarbon source depletion in this area).

Figures 4 through 8 show vertical and lateral transitions in soil-gas composition from high TPH and low O_2 concentrations to low TPH and high O_2 concentrations over distances of about 1 to 2 m. For example, for the 1.5-m separation between Locations 7 and 15, the subslab soil-gas changes from about 12% v/v O_2 and nondetect TPH to <1% v/v O_2 and 36 mg/L TPH. Figure 9 was prepared to evaluate the relationship between O_2 and TPH soil-gas concentrations at this site, and the two are inversely correlated. Elevated O_2 is generally found only in regions of nondetect TPH and depleted O_2 is almost always found in regions of elevated TPH.

This rapid attenuation with distance and inverse relationship between O_2 and TPH appears to be consistent with the hypothesis of aerobic biodegradation, as anticipated by the three-dimensional numerical simulations presented by Abreu and Johnson (2006) and as postulated by others to be occurring at their sites (Laubacher et al. 1997; McAlary et al. 2007).

The soil-gas distribution from the second sampling event was similar to that in the first sampling event. Again, areas beneath the building foundation were O_2 depleted, with the exception of a few locations. For example, location 16 installed in the high permeability utility trench showed higher O_2 concentrations, possibly as a result of the higher wind speeds at the time of sampling.

As discussed previously, the hydrocarbon composition of each sample was characterized in terms of mass percent of hydrocarbon vapors eluting between each n-alkane in the CH_4 to $C_{10}H_{22}$ range. Tables 3a to 3c present the results by sampling depth at subslab (0.15 m bgs), 0.3 m bgs (2 feet), and 0.6 m bgs (4 feet), respectively. The results indicate soil-gas composition generally dominated by CH_4 at all depths, with an average of about 20% to 60% (mass%) of the TPH. The remainder mostly consists of C_4 to C_9 compounds (30% to 70%) for TPH concentrations > 1 mg/L. It appears that many of the lower concentration samples are enriched in $>C_5H_{12}$ hydrocarbons, relative to the higher concentration source vapor composition. One possible explanation is that the smaller molecular weight $<C_5H_{12}$ compounds might be biodegrading preferentially relative to the heavier $>C_5H_{12}$ TPH components. However, other viable hypotheses may also exist.

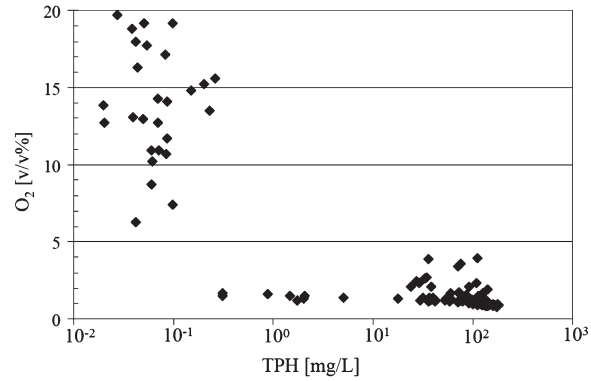

Figure 9. Relationship between TPH and O_2 concentrations in soil-gas samples collected during both sampling events. Note: there are 35 samples that had TPH concentrations at the detection limit of about 0.01 mg/L for the n-alkane TPH standards used in this study.

Implications for Pathway Assessment

As discussed previously, most current vapor intrusion pathway assessment guidance encourages a multiple-lines-of-evidence approach relying on ground water, deep soil-gas, subslab soil-gas, and indoor air concentrations.

Table 3a
Soil-Gas Carbon Range Composition at 0.15 m bgs (Subslab) Depth

Sampling Locations	Carbon Range Composition (mass in the range/total mass)											TPH (mg/L)
	CH_4	C1–C2	C2–C3	C3–C4	C4–C5	C5–C6	C6–C7	C7–C8	C8–C9	C9–C10	>C10	
5	0.00	0.00	0.00	0.00	0.16	0.25	0.22	0.21	0.07	0.09	0.00	0.03
16	0.04	0.00	0.00	0.03	0.07	0.16	0.25	0.20	0.06	0.08	0.11	0.05
3	0.48	0.00	0.00	0.00	0.07	0.12	0.14	0.08	0.03	0.03	0.05	0.14
7	0.00	0.00	0.00	0.00	0.06	0.10	0.23	0.22	0.12	0.04	0.25	0.15
14	0.63	0.00	0.00	0.00	0.05	0.08	0.11	0.07	0.04	0.02	0.00	31.4
15	0.56	0.00	0.00	0.00	0.06	0.10	0.13	0.08	0.04	0.02	0.00	35.85
1	0.47	0.00	0.00	0.00	0.10	0.18	0.18	0.06	0.00	0.00	0.00	38.17
8	0.52	0.00	0.00	0.01	0.09	0.15	0.15	0.06	0.01	0.00	0.00	50.70
11	0.64	0.00	0.00	0.00	0.08	0.10	0.11	0.05	0.01	0.00	0.00	54.77
12	0.50	0.00	0.00	0.01	0.10	0.14	0.15	0.08	0.02	0.01	0.00	58.14
9	0.51	0.00	0.00	0.00	0.10	0.14	0.15	0.07	0.02	0.01	0.00	58.47
2	0.68	0.00	0.00	0.00	0.08	0.10	0.10	0.04	0.01	0.00	0.00	59.53
17	0.44	0.00	0.00	0.00	0.07	0.12	0.20	0.12	0.03	0.01	0.00	66.66
13	0.44	0.00	0.00	0.01	0.11	0.17	0.17	0.08	0.02	0.01	0.00	90.01
10	0.42	0.00	0.01	0.01	0.11	0.16	0.19	0.09	0.02	0.01	0.00	103.05
4	0.41	0.00	0.00	0.01	0.10	0.17	0.20	0.09	0.02	0.01	0.00	109.34
6	0.40	0.00	0.00	0.01	0.10	0.17	0.20	0.09	0.02	0.00	0.00	110.35

Table 3b
Soil-Gas Carbon Range Composition at 0.6 m (2 feet) bgs Depth

Sampling Locations	Carbon Range Composition (mass in the range/total mass)											TPH (mg/L)
	CH_4	C1–C2	C2–C3	C3–C4	C4–C5	C5–C6	C6–C7	C7–C8	C8–C9	C9–C10	>C10	
N	0.12	0.00	0.00	0.00	0.04	0.15	0.10	0.09	0.19	0.26	0.04	0.04
L	0.04	0.00	0.00	0.00	0.00	0.06	0.10	0.12	0.13	0.16	0.38	0.04
16	0.00	0.00	0.00	0.03	0.11	0.22	0.27	0.18	0.06	0.03	0.10	0.05
5	0.47	0.00	0.00	0.00	0.09	0.16	0.10	0.03	0.06	0.05	0.05	0.07
K	0.02	0.00	0.00	0.03	0.05	0.12	0.23	0.17	0.09	0.15	0.15	0.08
I	0.02	0.00	0.00	0.00	0.03	0.17	0.26	0.14	0.06	0.04	0.27	0.09
M	0.12	0.00	0.00	0.00	0.07	0.17	0.25	0.11	0.06	0.10	0.12	0.10
F	0.01	0.00	0.00	0.00	0.04	0.12	0.24	0.21	0.12	0.10	0.17	0.19
J	0.01	0.00	0.00	0.01	0.06	0.13	0.32	0.24	0.12	0.07	0.02	0.26
E	0.23	0.00	0.00	0.00	0.08	0.14	0.24	0.14	0.06	0.06	0.04	0.70
B	0.19	0.00	0.00	0.01	0.16	0.28	0.22	0.11	0.02	0.01	0.01	8.24
G	0.10	0.00	0.00	0.00	0.09	0.21	0.33	0.20	0.06	0.01	0.00	26.15
7	0.98	0.00	0.00	0.00	0.00	0.01	0.00	0.00	0.00	0.00	0.00	27.45
15	0.53	0.00	0.00	0.00	0.06	0.10	0.14	0.08	0.05	0.03	0.01	29.38
8	0.57	0.00	0.00	0.01	0.07	0.13	0.14	0.07	0.01	0.00	0.00	34.96
14	0.57	0.00	0.00	0.00	0.06	0.09	0.13	0.09	0.04	0.02	0.00	35.77
H	0.51	0.00	0.00	0.01	0.09	0.14	0.15	0.08	0.02	0.01	0.00	37.14
9	0.42	0.00	0.00	0.01	0.10	0.15	0.19	0.10	0.03	0.01	0.00	73.09
3	0.49	0.00	0.00	0.01	0.10	0.17	0.17	0.06	0.01	0.00	0.00	76.54
17	0.39	0.00	0.00	0.00	0.07	0.12	0.21	0.15	0.05	0.01	0.00	79.24
C	0.40	0.00	0.00	0.01	0.10	0.19	0.21	0.08	0.01	0.00	0.00	100.42
12	0.41	0.00	0.00	0.01	0.12	0.19	0.18	0.08	0.01	0.01	0.00	108.45
D	0.35	0.00	0.00	0.01	0.15	0.21	0.20	0.08	0.01	0.00	0.00	111.10
10	0.42	0.00	0.00	0.00	0.11	0.16	0.19	0.09	0.02	0.01	0.00	112.08
6	0.37	0.00	0.00	0.01	0.10	0.18	0.22	0.10	0.01	0.00	0.00	115.53
13	0.36	0.00	0.00	0.01	0.11	0.19	0.21	0.10	0.01	0.00	0.00	118.58
1	0.43	0.00	0.00	0.01	0.12	0.19	0.18	0.06	0.01	0.00	0.00	122.76
11	0.34	0.00	0.00	0.01	0.10	0.16	0.23	0.11	0.03	0.01	0.00	125.91
2	0.37	0.00	0.00	0.01	0.11	0.18	0.22	0.10	0.02	0.00	0.00	130.83
4	0.38	0.00	0.00	0.01	0.13	0.19	0.19	0.08	0.01	0.00	0.00	145.30
A	0.35	0.00	0.00	0.01	0.13	0.22	0.21	0.07	0.01	0.00	0.00	166.65

Inherent in this approach is an assumption that the measured concentrations are sufficiently representative of the subsurface conditions.

This site illustrates potential challenges for the conventional assessment approaches for petroleum hydrocarbon sites. For example, the shallow subslab soil-gas distribution exhibits high spatial variability, with concentrations ranging from <0.1 to >100 mg/L. Random sampling of a few locations might not reveal the true range of concentrations. To place this in perspective, recall that Figures 4 to 6 were created with data from 17 sampling locations, and this number of samples is likely to be impractical for most pathway assessments. Even if one had precise knowledge of the subslab soil-gas distribution, it is not clear how it would be used to assess pathway significance without knowledge of the vapor entry points to the building and soil-gas flow rates through those points.

The soil-gas distribution data also point to the risks of relying on exterior sampling points because there are significant differences between exterior and interior soil-gas concentration and composition in the samples at shallow depths (equal or less than 2 feet bgs). This, again, is likely to be amplified at this site by the aerobically biodegradable nature of the petroleum hydrocarbons and the resultant rapid concentration attenuation in regions having elevated O_2 concentrations.

The soil-gas distribution data also suggest pathway assessment opportunities. For example, as shown in Figure 6, the spatial variability in the soil-gas distribution is small for soil-gas samples drawn from the source zone for both interior and exterior samples. Thus, contrary to subslab soil-gas spatial distribution characterization, only a few samples would characterize the source zone soil gas and exterior samples would be representative of conditions in the source zone below the slab. Thus, the data suggest a greater confidence and lower cost in the assessment of source zone concentrations vs. the assessment of subslab conditions. Having noted this, we do not yet know if this increased confidence and lower cost are also accompanied by similar or increased confidence in pathway assessment conclusions. For example, using source zone depth concentrations and composition may lead to overestimates of indoor impacts because the source zone concentrations and typical projection methods do not consider the aerobic biodegradation that will occur at sites where vapor transport occurs through well-oxygenated subsurface regions.

Table 3c
Soil-Gas Carbon Range Composition at 1.2 m (4 foot) bgs Depth

Sampling Locations	Carbon Range Composition (mass in the range/total mass)											TPH (mg/L)
	CH_4	C1–C2	C2–C3	C3–C4	C4–C5	C5–C6	C6–C7	C7–C8	C8–C9	C9–C10	>C10	
L	0.25	0.00	0.00	0.00	0.00	0.00	0.00	0.00	0.14	0.13	0.47	0.02
N	0.11	0.00	0.00	0.00	0.06	0.14	0.24	0.10	0.15	0.11	0.09	0.04
5	0.16	0.00	0.00	0.00	0.05	0.20	0.16	0.18	0.06	0.10	0.08	0.04
K	0.00	0.00	0.00	0.00	0.04	0.21	0.31	0.18	0.09	0.09	0.07	0.05
M	0.06	0.00	0.00	0.00	0.03	0.15	0.32	0.16	0.07	0.05	0.17	0.09
16	0.29	0.00	0.00	0.00	0.07	0.14	0.32	0.05	0.06	0.05	0.02	0.10
J	0.08	0.00	0.00	0.01	0.00	0.26	0.18	0.13	0.11	0.05	0.17	0.17
I	0.01	0.00	0.00	0.00	0.04	0.13	0.34	0.18	0.11	0.09	0.09	0.18
7	0.18	0.00	0.00	0.00	0.14	0.25	0.21	0.10	0.08	0.03	0.01	1.74
15	0.45	0.00	0.00	0.00	0.08	0.14	0.17	0.09	0.04	0.02	0.01	41.62
8	0.47	0.00	0.00	0.01	0.06	0.12	0.20	0.10	0.02	0.01	0.01	42.48
14	0.37	0.00	0.00	0.01	0.10	0.14	0.19	0.12	0.05	0.02	0.00	59.06
B	0.43	0.00	0.00	0.01	0.10	0.17	0.16	0.09	0.03	0.02	0.00	70.90
9	0.39	0.00	0.00	0.01	0.10	0.15	0.19	0.10	0.04	0.01	0.00	76.59
6	0.40	0.00	0.00	0.01	0.12	0.19	0.20	0.07	0.01	0.00	0.00	91.14
D	0.36	0.00	0.00	0.01	0.14	0.21	0.20	0.07	0.01	0.00	0.00	118.04
H	0.31	0.00	0.00	0.01	0.11	0.20	0.22	0.11	0.02	0.01	0.00	125.86
12	0.34	0.00	0.00	0.01	0.13	0.21	0.21	0.09	0.01	0.01	0.00	126.06
11	0.33	0.00	0.00	0.01	0.11	0.17	0.23	0.11	0.03	0.01	0.00	127.70
10	0.36	0.00	0.00	0.01	0.12	0.18	0.21	0.10	0.02	0.01	0.00	135.86
E	0.35	0.00	0.00	0.01	0.11	0.17	0.22	0.11	0.02	0.01	0.01	138.14
4	0.39	0.00	0.00	0.01	0.13	0.19	0.18	0.07	0.01	0.00	0.00	139.07
17	0.34	0.00	0.00	0.01	0.10	0.17	0.23	0.11	0.03	0.01	0.00	139.29
F	0.36	0.00	0.00	0.01	0.09	0.16	0.22	0.11	0.03	0.01	0.00	139.91
G	0.38	0.00	0.00	0.01	0.10	0.18	0.21	0.09	0.02	0.01	0.00	145.32
1	0.35	0.00	0.00	0.01	0.10	0.17	0.22	0.12	0.03	0.01	0.00	160.02
2	0.38	0.00	0.00	0.01	0.13	0.19	0.19	0.08	0.01	0.00	0.00	161.40
C	0.38	0.00	0.00	0.01	0.12	0.21	0.20	0.07	0.01	0.00	0.00	172.87
A	0.33	0.00	0.00	0.01	0.13	0.22	0.21	0.08	0.01	0.01	0.00	173.50
13	0.31	0.00	0.00	0.01	0.12	0.20	0.22	0.11	0.02	0.01	0.00	176.95
3	0.37	0.00	0.00	0.01	0.11	0.19	0.22	0.08	0.01	0.00	0.00	182.23

The TPH vs. O_2 graph prepared from site data and shown in Figure 9 indicates that O_2 might be used as a surrogate for screening sampling locations for aerobically biodegradable chemicals and for assessing the potential significance of petroleum hydrocarbon vapor intrusion. Combined with Figures 4 to 8, this plot suggests that well-oxygenated regions might be depleted of petroleum hydrocarbons where the oxygenated region is greater than 1 to 2 m thick. Future studies at other sites and employing methods with lower detection levels and individual hydrocarbon speciation would be needed to determine if this speculation holds true.

Supporting Information

The following supporting information is available for this article:

Figure S1. Comparison of soil-gas O_2 concentrations measured by O_2 sensors and GC-TCD during the first sampling event.

Please note: Blackwell Publishing is not responsible for the content or functionality of any supporting informations supplied by the authors. Any queries (other than missing information) should be directed to the corresponding author for the article.

References

Abreu, L.V.D., and P.C. Johnson. 2006. Simulating the effect of aerobic biodegradation on soil vapor intrusion into buildings: Influence of degradation rate, source concentration and depth. *Environmental Science and Technology* 40, no. 7: 2304–2315.

Abreu, L.V.D., and P.C. Johnson. 2005. Effect of vapor source-building separation and building construction on soil vapor intrusion as studied with a three-dimensional numerical model. *Environmental Science and Technology* 39, no. 12: 4550–4561.

Fischer, M.L., A.J. Benley, K.A. Dunkin, A.T. Hodson, W.W. Nazaroff, R.G. Sextro, and J.M. Daisey. 1996. Factors affecting indoor air concentrations of volatile organic compounds at a site of subsurface gasoline contamination. *Environmental Science and Technology* 30, no. 10: 2948–2957.

Fitzpatrick, N.A., and J.J. Fitzgerald. 2002. Evaluation of vapor intrusion into buildings through a study of field data. *Soil & Sediment Contamination* 11, no. 4: 603–623.

Hers, I., R. Zapf-Gilje, D. Evans, and L. Li. 2002. Comparison, validation, and use of models for predicting indoor air quality

from soils and groundwater contamination. *Soil & Sediment Contamination* 11, no. 4: 491–527.

Hers, I., and R. Zapf-Gilje. 1998. Canadian consortium research project-field validation of soil gas transport to indoor air pathway. In *Proceedings of the Petroleum Hydrocarbons and Organic Chemicals in Ground Water: Prevention, Detection, and Remediation Conference*, 1–10. Houston, Texas, November 11–13, 1998.

Johnson, P.C., R.A. Ettinger, J. Kurtz, R. Bryan, and J.E. Kester. 2002. Migration of soil-gas vapors to indoor air: Determining vapor attenuation factors using a screening-level model and field data from the CDOT-MTL, Denver, Colorado. API Soil and Groundwater Task Force Bulletin No. 16. Washington, D.C.: American Petroleum Institute.

Johnson, P.C., and R.A. Ettinger. 1991. Heuristic model for predicting the intrusion rate of contaminant vapors into buildings. *Environmental Science and Technology* 25, no. 8: 1445–1452.

Laubacher, R.C., P. Bartholomae, P. Velasco, and H.J. Reisinger. 1997. An evaluation of the vapor profile in the vadose zone above a gasoline plume. In *Proceedings of the Petroleum Hydrocarbons and Organic Chemicals in Ground Water: Prevention, Detection, and Remediation Conference*, 396–409. Houston, Texas, 1997.

Little, J.C., J.M. Daisey, and W.W. Nazaroff. 1992. Transport of subsurface contaminants into buildings: An exposure pathway for volatile organics. *Environmental Science and Technology* 26, no. 11: 2058–2066.

McAlary, T., Nicholson, P., Bertrand, D., Abreu, L., and Ettinger, R. 2007. A case study on the influence of aerobic biodegradation on vapor intrusion at a former refinery property. In *Proceedings of AWMA Conference on Vapor Intrusion: Learning From Challenges*, 196–212. Providence, RI, September 26–28, 2007.

Nazaroff, W.W., S.R. Lewis, S.M. Doyle, B.A. Moed, and A.V. Nero. 1987. Experiments on pollutant transport from soil into residential basement by pressure-driven airflow. *Environmental Science and Technology* 21, no. 5: 459–466.

Nazaroff, W.W., H. Feustel, A.V. Nero, K.L. Revzan, and D.T. Grimsrud. 1985. Radon transport into a detached one-story house with a basement. *Environmental Science and Technology* 19, no. 1: 31–46.

USEPA. 2004. User's guide for evaluating subsurface vapor intrusion into buildings. Washington, D.C.: U.S. Environmental Protection Agency.

USEPA. 2002. Draft guidance for evaluating the vapor intrusion to indoor air pathway from groundwater and soils (subsurface vapor intrusion guidance). *Federal Register* 67, no. 230: 132–133.

Biographical Sketches

***Hong Luo**, corresponding author, is a Ph.D candidate of civil and environmental engineering in the Ira A. Fulton School of Engineering at Arizona State University. She can be reached at hong.luo@asu.edu.*

***Paul R. Dahlen**, Ph.D., is an assistant professor of research in environmental engineering with Arizona State University. He can be reached at 1711 S. Rural Rd., ECG-252, Tempe, AZ 85287; (480) 965-0055; paul.dahlen@asu.edu.*

***Paul C. Johnson**, Ph.D., is a professor of civil and environmental engineering in the Ira A. Fulton School of Engineering at Arizona State University. His research and professional activities focus on gaining a better understanding the migration and fate of chemicals in the subsurface with application to remediation and risk assessment. He can be reached at paul.c.johnson@asu.edu.*

***Tom Peargin**, is a staff hydrogeologist with Chevron Energy Technology Company, where he provides technical support to Chevron's international operations, including the development and testing of practical guidelines for site assessment, risk pathway assessment, remediation, and monitoring activities. He can be reached at TPeargin@chevron.com.*

***Todd N. Creamer**, M.S., is a senior geologist with Geosyntec Consultants, Inc. He can be reached at 289 Great Road, Suite 105, Acton, MA 01720; (978) 263-9588; tcreamer@geosyntec.com.*